A Generalized Two-Factor Square-Root Model to Forecast Cost and Volatility Of Natural Catastrophes

Giuseppe Orlando[1a], Michele Bufalo[b]

[a] *Università degli Studi di Bari Aldo Moro - Department of Economics and Finance, Via C. Rosalba 53, Bari, I-70124 Italy, Tel. +39 080 5049218, giuseppe.orlando@uniba.it*
[b] *Università degli Studi di Roma "La Sapienza" - Department of Methods and Models for Economics, Territory and Finance, Via del Castro Laurenziano 9, Roma, I-00185, Tel. +39 06 49766903, michele.bufalo@uniroma1.it*

Abstract

In this work we intend to forecast (from 1 to 15 years horizon) the expected value of financial losses due to natural catastrophes as well as their volatility where the latter is potentially responsible for dramatic swings of Profit and Loss (P&L) for those companies affected by unexpected events. To do that, we developed a new generalized two-factor square-root model that enables us to link together occurrences and volatility through correlated Brownian motions. In addition, by means of a Generalized Pareto Distribution (GPD), we forecast the maximum loss in terms of Value at Risk (VaR) for each type of natural disaster. Finally, the accuracy of our results is checked by a comparison with four baseline models and validated by a backtesting analysis. This methodology is primarily designed for insurance companies that need to avoid erratically reserves but it could be extended to any firm that is exposed to extreme events and intends to preserve a stable cash flow to the shareholders.

Keywords: Forecasting; Natural disasters; two-factor square-root model; Generalized Pareto Distribution; model validation
JEL Classification: C53; C52; G22
2010 MSC: 62P05; 91G05; 91G70

[1]Corresponding author.

1. Introduction

The purpose of the present work is forecasting the financial losses caused by some natural catastrophes as well as their volatility from short-term (1 year) to long-term horizon (up to 15 years). In particular, we want to predict the expected value of the above-mentioned quantities which are of high importance, since it is their great variability and non-Gaussian behaviour that makes any sophisticated model fallacious to the point that simple models, such as autoregressive or moving average, are more successful. Here we propose a new two-factor model where mean and variance are correlated processes. This is new in literature and it is difficult to implement, to the point that there are no closed form solutions Brigo and Mercurio (2006). Based on the model, we are able to calculate an upper bound that follows a Pareto distribution and represents the VaR for backtesting. This approach is new in literature as well. Being able to forecast the interaction between losses and volatility is very important for stabilizing the P&L. The proposed methodology is on the edge between banking and insurance. It has been expressly designed for insurers and reinsurers but applies as well to banks and other companies when exposed to dramatic changes of a given line of business (LOB) due to unexpected events.

To begin with, we denote by X_t the amount of the losses L_t at time t, i.e.,

$$X_t = \sum_{h=1}^{t} L_h.$$

To measure the variability of a time series of losses, $\{X_t\}$, we compute the percentage change defined as

$$\frac{X_t - X_{t-1}}{X_{t-1}}.$$

Natural catastrophes (often abbreviated as NatCat) encompasses property policies such as earthquake and land slide failure, primary and excess storm and flood insurance, etc. Table 1 shows the magnitude of those percentage (of order 10^4) over five natural disasters with higher impact (the dataset is described in Section 3.1). Note that volatilities are of order of magnitude between 10^3 and 10^4 which makes complicates any forecasting attempt. Therefore, due to the high variability of time series and as commonly done in finance, we are going to consider log returns (i.e. $\ln(X_t/X_{t-1})$) only.

Further, in Figure 1 the log returns are plotted for the five chosen natural disasters, whereas Table 2 reports the sample mean and standard deviation of log returns as well as the skewness and kurtosis of their empirical distribution. Observe that

	Maximum of Loss Returns				
	Earthquake	**Storm**	**Flood**	**Drought**	**Ext. Temp.**
Perc. change ($\cdot 10^4$)	1.97%	0.04%	1.01%	0.03%	0.26%
Perc. change of log returns	3.65%	12.56	22.25%	23.25%	9.72%

Table 1: Maximum of $X_t/X_{t-1} - 1$ and of $\ln(X_t/X_{t-1})$ due to natural disaster (annual data from 1900 to 2020).

the logarithms showed in Figure 1 are always positive being the amount of losses an increasing quantity in time. Obviously, it is a different behaviour from the Gaussian distribution.

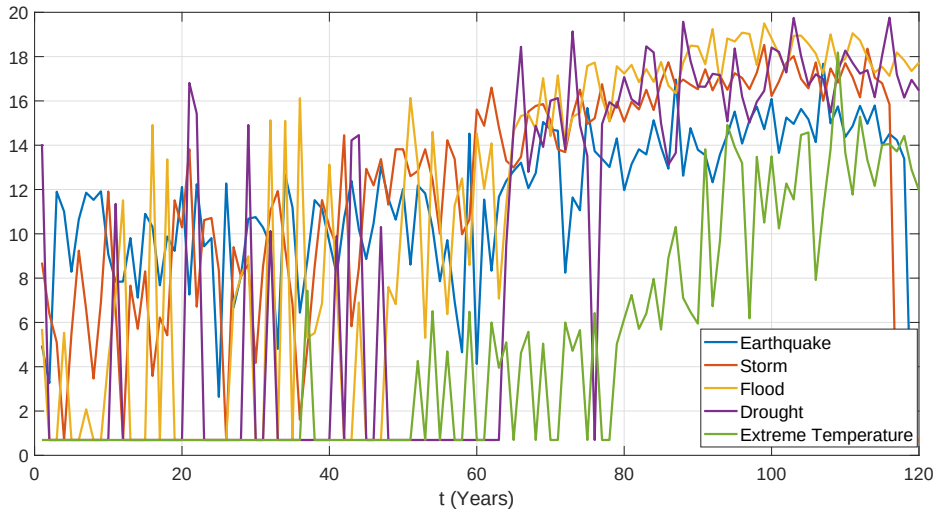

Figure 1: Logarithms of losses due to natural disasters (annual data from 1900 to 2020).

	Earthquake	**Storm**	**Flood**	**Drought**	**Ext. Temp.**
Mean	11.50	12.07	11.30	9.08	4.88
Std. Dev.	3.38	5.03	7.01	7.80	5.15
Skewness	-0.92	-0.78	-0.49	-0.07	0.81
Kurtosis	3.80	2.57	1.61	1.13	2.23

Table 2: Four indices of log returns empirical distribution (annual data from 1900 to 2020).

Modeling natural catastrophes evolved in the late 1980s. The Hurricane Andrew in 1992 and the Northridge earthquake in 1994 put further pressure on companies to more accurately analyze, write and price natural catastrophe risk. Because of global warming, frequency and severity of some climate-related events such as flood, drought, storms, etc. evidenced the limits of catastrophe models as they underestimated the losses. Estimates used to rely on long-term trends but, in the wake of of the record hurricane seasons and amid predictions of increased storm activity, modelers began to incorporate near-term projections of loss. These near-term models started to reflect five-year outlooks. However, even those predictions, in some cases, were not sufficient and new methods were developed to forecast the severity of next record insured loss to property caused by natural catastrophic events Hsieh (2004). That is the path we intend to follow.

As detailed in next section, there are many stochastic models able to describe persistent jumps and high levels of volatility. Over the last years, we have developed our own methodology Orlando et al. (2018), 2019a, 2019b, 2019c, on which we have built a new model expressly designed for describing natural disasters. However, due to the high variability previously illustrated, we decided to adopt a two-factor model. In this work we intend to show that our model is not only able to predict the average losses and their volatility but, also, it is able to calculate a proper upper bound. The latter, in our framework, follows a Pareto distribution and represents our Value at Risk (VaR).

This paper is organized as follows. Next Section resumes the existing literature and gives an account of the reasons we have selected the proposed model. Section 3 is about materials, methods and techniques. In there we start by describing the data source followed by the proposed model. Backtesting analysis for model validation concludes the Section. Numerical results are illustrated in Section 4. Finally, Section 5 contains the conclusions and the Appendix A contains graphical evidences on the validity of the proposed model.

2. Literature review and model selection

Natural disasters are complex dynamic systems with, sometimes, disastrous impacts on environment and people. Both frequency of occurrences and severity grow with time because of climate change and increasing human population. They are nonlinear and characterized by low correlation and high intermittency Jin et al. (2008). Typical tools for time series analysis are not of easy application because of discontinuity and different cycles mutually nested Jin et al. (2008). For instance a large set of models and tests are not applicable because they are based on Gaussian

behaviour. The same applies to nonlinear techniques such as ARIMA that relies on assumptions such as stationarity, invertibility and independence of residuals Povinelli (2000). More successful application have ARCH/GARCH models because, on long-term horizons, they display weak persistency as "the time correlation disappears and a simple uncorrelated Itô process is recovered" Carbone et al. (2004). The squared form of the lagged shocks, however, disables the ability to deal with asymmetric volatility due to different effect that positive or negative perturbations may have Zivot (2009).

A different kind of models, but explicitly designed for earthquakes, are based on the Utsu (1970) framework in which a combination of a strong main shock and after-shocks is considered to assess the total damage (see for example Cai et al. (2020)).

Point process such as Hawkes process are widespread in finance as they are able of modelling temporal events characterized by self-exciting properties (for a survey see Bacry et al. (2015) and Hawkes (2018)). They have been used for modelling order-book events, risk contagion modeling, optimal execution strategies, etc. In insurance they can be employed for modelling earthquake swarms Ogata (1988) or mortality risk Cox et al. (2010). Multivariate Hawkes processes Embrechts et al. (2011) are expressly designed to model multiple correlated sequences, where the occurrence of an event in a sequence may influence the occurrence of new events in another sequence. However, those processes may either fail in capturing the mutual influence between processes or may become computational inhibitive Hall and Willett (2016), Eichler et al. (2017), Shang and Sun (2019). For this reason, in our quest for jointly modelling expected losses and volatility for any kind of natural disaster, we had decided to not pursue on this pathway.

As mentioned in the Introduction, in this work we want to follow a new path based on our previous research on financial time series, but in order to do so, we need first to characterize natural disaster dynamics in terms of persistence and randomness. Persistency (or trend reinforcing) is when, in a time series, next value is more likely the same as the current value. For analysing that, we recur to the Hurst exponent (H_e) Hurst (1956) which varies between 0 and 1. Low levels of H_e indicate that the dynamics is anti-persistent and anti-correlated, H_e around $= 0.5$ implies randomness, high values indicate persistent and correlated dynamics.

The Hurst exponent "is robust with few assumptions about the underlying system, it has broad applicability for time series analysis" Qian and Rasheed (2004) moreover is a "robust statistic for testing the presence of noncyclic long run statistical dependence" Mandelbrot and Wallis (1969). For those reasons the H_e has been employed in various fields. For instance, Mandelbrot and Van Ness (1968) applied it

when modelling, by means of fractional Brownian motions, strong interdependence between distant samples in natural time series.

In finance the Hurst exponent is around 0.5 Nawrocki (1995), Qian and Rasheed (2004), but it varies a lot depending on the market sentiments leading to "some episodes alternating low and high persistent behavior" Alvarez-Ramirez et al. (2008) occurring in correspondence of downturns.

With regard to natural disaster the H_e is around 0.24, which "indicates that these time series are fractal and relatively long-term" anti-persistent Jin et al. (2008). On our end we confirm what has been reported in literature (see Table 3).

A low level of the Hurst exponent indicates that the strength of mean-reverting does increase. For this reason we selected a generalized two-factor square-root model that, in our opinion, matches the above specified features. By doing that we take some inspiration from observing electricity spot prices. In that context, for example, an Ornstein-Uhlenbeck process, i.e. a mean-reverting drift damping model, has been used for modelling volatility persistence and anti-correlations Rypdal and Løvsletten (2013). By drawing this parallel, for forecasting losses due to natural disasters, we link up with the set of tools available for financial analysis and risk management.

Earthquake	**Storm**	**Flood**	**Drought**	**Ext. Temp.**
0.0887	0.2026	0.1287	0.1528	0.0964

Table 3: Hurst exponent for log-losses of natural disasters.

As just mentioned, there is a wide range of models available in financial literature. As we need to model levels, volatilities and their interdependencies, we exclude unifactorial models. In addition, as there is a trade-off between the increased benefit of having a large number of state variables and issues caused by estimations, overfitting and so on, we limit ourselves to the class of two-factor models. On those models literature is abundant Rouah (2013), Tsuchiya (2019), Ewald et al. (2019).

The Heston model 1993, for example, may suit well because it describes the evolution of an asset jointly with its volatility. However, as noted by Heston himself, an increase in the volatility of volatility can capture the kurtosis of spot returns but not the skewness. Therefore, "in order to capture the skewness, it is crucial to also include the properly specified correlation between the volatility and the spot exchange rate of returns" Ahlip et al. (2017). As in our time series, kurtosis is much higher than skewness (see Table 2) this shortfall is crucial.

The so-called two-factor Gaussian models were introduced by Hull and White 1994 and then extended by Brigo and Mercurio with the G2++ model 2006. They

first determine a time homogeneous two-factor short rate dynamics and then, they add a deterministic shift function to fit the initial term structure of interest rates. However, "the obtained results are rather clumsy and not intuitive, which means that a special care has to be taken for their correct numerical implementation" Acar and Natcheva-Acar (2009).

Another class of two-factor models is the one introduced by Longstaff and Schwartz 1992, which belongs to the class of stochastic mean and stochastic volatility model. Within the proposed framework, Longstaff and Schwartz approached interest rate volatility and term structure modelling by linking up yields on volatility. This framework performs better than the GARCH model Bollerslev (1986) because the addition of the volatility as a second state variable allows more freedom in modelling humps, troughs, and interconnectedness between levels and volatility. Empirical evidence found that the short rate exhibits volatility clusters which can be well approximated by stochastic volatility Faff and Treepongkaruna (2013). More recently, Christoffersen et al. (2009) modelled levels by a stochastic high mean reversion factor, and correlations between returns and variance by a second factor with lower mean reversion. Similarly, Recchioni and Sun (2016) modelled asset price dynamics by a two-factor model where the first factor represents stochastic interest rates and the second one stochastic volatility. On pricing and risk in natural gas markets Kohrs et al. (2019) proposed a multidimensional variant of the Longstaff–Schwartz model for deriving options' properties under realistic price dynamics.

Other models, commonly used for studying the tail behaviour of distribution, are based on the extreme value theory (EVT). Within the EVT framework, we consider the generalized Pareto distribution (GPD) introduced by Pickands III (1975). A classical reference is Coles et al. (2001) who introduces the theoretical framework of extreme value models and the statistical inferential techniques. GPD has applications in a number of fields, including epidemiology Chen et al. (2015), non-life insurance Hanafy et al. (2020), environmental extreme events Chavas et al. (2013), Martins et al. (2020), etc. For this reason we include it between the baseline models against which we intend to run our analysis.

The last class of models we consider as baseline is the generalized linear model (GLM) Nelder and Wedderburn (1972) which allows for response variables to have error distribution models other than a normal distribution. GLM has extensive application in insurance. For example claim sizes, frequencies and occurrences of claims do not have normal outcomes. Furthermore, the link between outcomes and risk drivers is multiplicative rather additive De Jong and Heller (2008). Thus the distribution of the response is chosen from the exponential family so that the response can be heteroskedastic.

In this work, in a quite different context, we draw inspiration from the above mentioned literature when dealing with natural disasters.

3. Materials, methods and techniques

This Section is partitioned as follows. After mentioning the dataset used for numerical results in Section 3.1, we introduce our two-factor square-root model to describe the dynamics of log-losses and their volatility in Section 3.2. Further, two baseline models for comparison and benchmarking are considered in Section 3.3. The numerical simulation and the parameter calibration of the proposed model are explained in Section 3.4. Expected value predictions of log-losses and their volatility are obtained by providing, via a Generalized Pareto Distribution (GPD), a maximum threshold estimate of log-losses in terms of Value at Risk (VaR). Next, measures of forecasting accuracy are defined in Section 3.5, and, finally, the most popular backtests used by financial institutions are considered in Section 3.6 to validate our model based on VaR exceedances.

3.1. Dataset

Our dataset is from the Emergency Events Database (EM-DAT) hosted at the Centre for Research on the Epidemiology of Disasters (CRED). The EM-DAT database contains the "world's most comprehensive data on the occurrence and effects of more than 23,000 technological and natural disasters from 1900 to the present day" CRED (2020). Frequency of data is on an annual basis. For our convenience we have decided to focus on five natural disasters with higher impact, namely earthquake, storm, flood, drought and extreme temperature (see Figure 2).

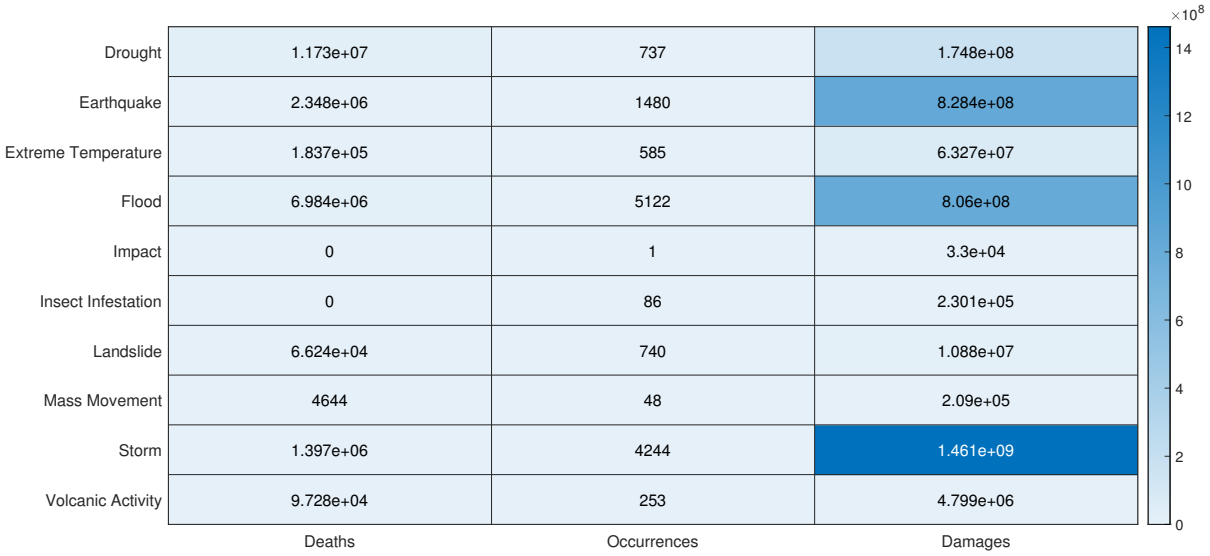

Figure 2: Sum of deaths, occurrences and total damages (US$) of natural disasters (1900-2020).

3.2. A generalized two-factor square-root model

To introduce our generalized two-factor square-root model, let us start by denoting with $(x_t)_{t\geq 0}$ and $(\sigma_t)_{t\geq 0}$, respectively, the logarithm of financial losses due to natural disasters and the corresponding volatility. Assume that the dynamics of these processes, defined on a given probability space $(\Omega, \mathcal{F}, \mathbb{P})$, where $\mathbb{P}$ is the objective probability measure, evolves like a generalized two-factor square-root model defined as follows

$$\begin{cases} dx_t = k(\theta - x_t)dt + \omega\sqrt{x_t\sigma_t}\, dW_t^x \qquad (x_0 \geq 0) \\ d\sigma_t = \delta(\gamma - \sigma_t)dt + \eta\sqrt{\sigma_t}\, dW_t^\sigma \qquad (\sigma_0 \geq 0), \end{cases} \tag{1}$$

where $(W_t^x)_{t\geq 0}$ and $(W_t^\sigma)_{t\geq 0}$ are two correlated Brownian motions, i.e.,

$$dW_t^x dW_t^\sigma = \rho\, dt \qquad (t \geq 0).$$

We can write

$$W_t^x = \rho W_t^\sigma + \sqrt{1-\rho^2}\, B_t, \tag{2}$$

where $(B_t)_{t\geq 0}$ is a standard Brownian motion independent of $(W_t^\sigma)_{t\geq 0}$.
Assume

$$2\delta\gamma > \eta^2, \qquad 2k\theta > \omega^2\sigma,$$

so that the state-spaces of the processes $(\sigma_t)_{t\geq 0}$ and $(x_t|\sigma_t = \sigma)_{t\geq 0}$ (with $\sigma > 0$) are both equal to $\mathbb{R}_+$.

Two-factor models like the one in Eq. (1) have advantages and disadvantages that should be considered in terms of the intended use before to select one of them. For example, in order to preserve the analytical tractability, the CIR2++ has set $\rho = 0$. Without that, it is no possible to compute analytically bond prices and rates starting from the short-rate factors. This because the square-root non-central chi-square processes "do not work as well as linear-Gaussian processes when adding nonzero instantaneous correlations" Brigo and Mercurio (2006). Another feature of the CIR2++ is that it can maintain positive rates through reasonable restrictions on the parameters and that it has fatter tails than the Gaussian distribution in G2++. In fact, in the CIR2++ model, the distribution of the short rate is the result of the sum of two independent noncentral chi-square variables. However, the G2++ model is more analytically tractable and easier to implement, thus it is more suitable for practical applications.

A possible way to reduce the negative impact of the non-zero correlation ρ on the numerical tractability is given by the following result.

Proposition 3.1. *With refer to* (1)*, consider the functions*

$$g(y) = \int_{x_0}^{y} \frac{1}{\sqrt{u}}\, du, \qquad f(y) = \frac{\omega}{\eta}(y - \sigma_0) \qquad (y \in \mathbb{R}_+). \tag{3}$$

Then, the system of SDE's (1) *is equivalent to*

$$\begin{cases} d\big(g(x_t) - \rho f(\sigma_t)\big) = h(x_t, \sigma_t)dt + \omega\sqrt{\sigma_t(1-\rho^2)}\, dB_t \\ d\sigma_t = \delta(\gamma - \sigma_t)dt + \eta\sqrt{\sigma_t}\, dW_t^{\sigma}, \end{cases} \tag{4}$$

where

$$h(x_t, \sigma_t) = \frac{k(\theta - x_t)}{\sqrt{x_t}} - \frac{\omega^2\sigma_t}{2} - \frac{\rho\omega\delta(\gamma - \sigma_t)}{\eta}. \tag{5}$$

Proof. By virtue of the Ito-Doeblin formula (see, e.g., (Shreve 2004, Section 4.4.2)) we get

$$dg(x_t) = \frac{1}{\sqrt{x_t}}dx_t - \frac{1}{2x_t\sqrt{x_t}}(dx_t)^2 = \left(\frac{k(\theta - x_t)}{\sqrt{x_t}} - \frac{\omega^2\sigma_t}{2}\right)dt + \omega\sqrt{\sigma_t}\, dW_t^x, \tag{6}$$

and

$$df(\sigma_t) = \frac{\omega}{\eta}\, d\sigma_t = \frac{\omega\delta(\gamma - \sigma_t)}{\eta}dt + \omega\sqrt{\sigma_t}\, dW_t^{\sigma}. \tag{7}$$

If substitute (2) and (7) in (6), obtain

$$dg(x_t) = \left(\frac{k(\theta - x_t)}{\sqrt{x_t}} - \frac{\omega^2\sigma_t}{2}\right)dt + \omega\sqrt{\sigma_t}\,(\rho dW_t^\sigma + \sqrt{1-\rho^2}\,dB_t) =$$

$$\left(\frac{k(\theta - x_t)}{\sqrt{x_t}} - \frac{\omega^2\sigma_t}{2} - \frac{\rho\omega\delta(\gamma - \sigma_t)}{\eta}\right)dt + \rho df(\sigma_t) + \omega\sqrt{\sigma_t(1-\rho^2)}\,dB_t,$$

i.e.,

$$d\big(g(x_t) - \rho f(\sigma_t)\big) = h(x_t, \sigma_t)dt + \omega\sqrt{\sigma_t(1-\rho^2)}\,dB_t.$$

□

The above function g in (3) represents the so-called *Lamperti's transformation* which reduces to 1 the diffusion term of $(x_t)_{t\geq 0}$. Proposition 3.1 introduces a new auxiliary process

$$p_t := g(x_t) - \rho f(\sigma_t) \qquad (t \geq 0) \tag{8}$$

with dynamics

$$dp_t = h(x_t, \sigma_t)dt + \omega\sqrt{\sigma_t(1-\rho^2)}\,dB_t,$$

or, equivalently,

$$p_t = p_0 + \int_0^t h(x_s, \sigma_s)\,ds + \omega\sqrt{1-\rho^2}\int_0^t \sqrt{\sigma_s}\,dB_s,$$

where $p_0 = g(x_0) - \rho f(\sigma_0) \geq 0$. In particular, the stochastic part of $(p_t)_{t\geq 0}$ is not correlated with those of $(\sigma_t)_{t\geq 0}$. This fact allows a fast and independent simulation of the process $(x_t)_{t\geq 0}$; indeed, one can simulate $(\sigma_t)_{t\geq 0}$ and $(p_t)_{t\geq 0}$ separately and finally may compute $(x_t)_{t\geq 0}$ as

$$x_t = g^{-1}(p_t + \rho f(\sigma_t)) \tag{9}$$

(being g an invertible function).
In view of the forecast analysis (see Section 4), another helpful result concerning $(p_t)_{t\geq 0}$ is given below.

Proposition 3.2. *The conditioned auxiliary process* $(p_t|\sigma_t = \sigma)_{t\geq 0}$ $(\sigma > 0)$ *satisfies the strong Markov property.*

Proof. It is simple to see that the infinitesimal generator of $(x_t|\sigma_t = \sigma)_{t\geq 0}$ is a one-dimensional time-homogeneous operator, given by

$$\mathcal{L}^x u(x) = \frac{\omega^2\sigma\,x}{2}\frac{\partial^2 u(x)}{\partial x^2} + k(\theta - x)\frac{\partial u(x)}{\partial x},$$

for any dummy variable $x \in \mathbb{R}_+$ and for any u of class C_0[2].
Analogously, the infinitesimal generator of $(p_t|\sigma_t = \sigma)_{t\geq 0}$ is given by

$$\mathcal{L}^p u(p) = \frac{\omega^2 \sigma (1-\rho^2)}{2} \frac{\partial^2 u(p)}{\partial p^2} + h(p,\sigma) \frac{\partial u(p)}{\partial p},$$

for any $p \in \mathbb{R}$, $u \in C_0(\mathbb{R}_+)$, with h defined in (5).
Following Goldstein et al. (2016), the operator $\mathcal{L}^x$, with domain

$$D(\mathcal{L}^x) = \{u \in C_0(\mathbb{R}_+) \cup C^2(\mathbb{R}_+) | \mathcal{L}^x u \in C_0(\mathbb{R}_+)\},$$

generates a Feller semigroup on $C_0(\mathbb{R}_+)$ (see Engel and Nagel (2001), Goldstein (1985)). Moreover, there exists an isomorphism

$$\Psi := g - \rho f$$

which links the two variables x, p (and maps $\mathbb{R}_+$ in $\mathbb{R}$), so that also the operator $\mathcal{L}^p$, with domain

$$D(\mathcal{L}^p) = \{u \in C_0(\mathbb{R}) \cup C^2(\mathbb{R}) | \mathcal{L}^p u \in C_0(\mathbb{R})\},$$

generates a Feller semigroup on $C_0(\mathbb{R}_+)$ (see (Bufalo et al. 2019, Lemma A.2) and (Engel and Nagel 2001, Chapter II, Section 2.a)). This concludes the proof, since any stochastic Feller process (i.e., a stochastic process whose infinitesimal generator, with its domain, generates a Feller semigroup) verifies the strong Markov property (see, also Böttcher et al. (2013), Oksendal (2013) and Taira (1984)). □

3.3. Baseline models

In this Section four baseline models for comparison and benchmarking are considered as alternative candidates to Eq. (1) for modelling log-losses of natural disasters. Namely, the first-order autoregressive AR(1) model, the two-factor Gaussian model G2++, the extreme vale distribution model and the nonlinear regression model. The AR(1) is pretty good in predicting the average loss and volatility of the stochastic process when more sophisticated models fail. The other three models are often used in insurance and finance for modeling and forecasting stochastic processes as mentioned in Sec. 2.

[2] $C_0(\mathbb{R}_+)$ denotes the Banach space of all the continuous and real-evaluated functions vanishing at infinity

3.3.1. The first-order autoregressive AR(1) model

The AR(1) model is a representation of a short-memory random process satisfying the following equation:

$$Y_{t+1} = c + \Phi Y_t + \varepsilon_{t+1}.$$

The output random variable Y_{t+1} is assumed to depend linearly only on its own previous value Y_t and on the current value of a white noise process ε_t with zero mean and constant variance σ_ε^2. The process is stationary if the parameter $\varphi \in (0, 1)$.

The AR(1) model has been already used in modelling and understanding persistence of climate variability Vyushin et al. (2012). Moreover, it can be considered as the discrete-time analogue of the mean-reverting Ornstein-Uhlenbeck (OU) process

$$dY_t = \chi(\mu - Y_t)dt + \lambda dW_t.$$

Indeed, when the Ornstein-Uhlenbeck process is sampled at equally spaced time intervals $[t, t + \Delta]$, we get

$$Y_{t+\Delta} = c + \Phi Y_t + \varepsilon_{t+\Delta},$$

with

$$\Phi = e^{-\chi\Delta}, \quad c = (1 - \Phi)\mu, \quad \varepsilon_{t+\Delta} \sim N\left(0, \frac{\lambda^2}{2\chi}(1 - \Phi^2)\right).$$

The conditional distribution of the OU process is normal with parameters

$$\mathbb{E}[Y_{t+n\Delta}|Y_t] = \mu(1 - \Phi^n) + Y_t\,\Phi^n$$

and

$$\text{Var}\,(Y_{t+n\Delta}|Y_t) = \frac{\lambda^2}{2\chi}(1 - \Phi^{2n}).$$

3.3.2. The G2++ model

The G2++ model is a two-factor Gaussian model where the state process is given by the sum of two correlated Gaussian factors plus a deterministic function that is properly chosen so as to exactly fit the real observed data. The model is analytically quite tractable as explicit formulas for its distribution and moments can be readily derived; for these reasons, Gaussian models like this G2++ model are very useful in practice (for more details see (Brigo and Mercurio 2006, Chapter IV)). Under this model the principal process Y_t is expressed as the sum

$$Y_t = r_t + q_t + \varphi(t),$$

where the processes $\{r_t\}_{t\geq 0}$ and $\{q_t\}_{t\geq 0}$ satisfy

$$\begin{cases} dr_t = -a\, r_t dt + \psi\, dW_t^r \\ dq_t = -b\, q\, dt + \zeta\, dW_t^q \end{cases} \tag{10}$$

with $dW_t^r dW_t^q = \rho\, dt$ and a, ψ, b, ζ are positive constants. In particular, the model fits the observed data if and only if (Brigo and Mercurio 2006, Corollary 4.2.1))

$$\varphi(t) = f_s(t) + \left(\frac{\psi}{2a_s}\big(1 - e^{-a(t-s)}\big)\right)^2 + \left(\frac{\zeta}{2b}\big(1 - e^{-b(t-s)}\big)\right)^2 + \rho\frac{\psi\zeta}{a\, b}\big(1 - e^{-a(t-s)}\big)\big(1 - e^{b(t-s)}\big),$$

where $f_s(t)$ denotes the instantaneous forward value of Y_t in t, computed at time $s < t$.

Denoted by $\mathcal{F}_t$ the sigma-field generated by the pair (r_t, q_t) at time t, it can be shown that for any $0 \leq s < t$, X_t conditional on $\mathcal{F}_s$ is normally distributed with mean

$$\mathbb{E}[Y_t|\mathcal{F}_s] = r_s e^{-a(t-s)} + q_s e^{-b(t-s)} + \varphi(t), \tag{11}$$

and variance

$$\text{Var}\,(Y_t|\mathcal{F}_s) = \frac{\psi^2}{2a}\big(1 - e^{-2a(t-s)}\big) + \frac{\zeta^2}{2b}\big(1 - e^{-2b(t-s)}\big) + 2\rho\left(\frac{\psi\,\zeta}{a+b}\right)\big(1 - e^{-(a+b)(t-s)}\big). \tag{12}$$

3.3.3. The extreme value distribution model (EVM)

Extreme value distributions are very popular in finance as they are useful to model extreme events that are not captured by other distributions like the Gaussian whose tails decay exponentially fast.

Given the location parameter a_1 and scale parameter a_2, the probability density function for the extreme value distribution

$$y = f(x|a_1, a_2) = \frac{1}{a_2} e^{(x-a_1)/a_2 - e^{(x-a_1)/a_2}}.$$

It can be observed that if X has a Weibull distribution with parameters b_1 and b_2, then $\log X$ has an extreme value distribution with parameters $a_1 = \log b_1$ and $a_2 = 1/b_2$.

3.3.4. Generalized linear model (GLM)

The last baseline model that we introduce for comparison is the generalized linear model (GLM) that we use for nonlinear prediction (NLP)

$$y = c_1 + c_2 e^{-c_3 x} \tag{13}$$

on which we have performed a nonlinear least squares regression. Eq. (13) is consistent with the G2++, is an industry standard De Jong and Heller (2008), Ohlsson and Johansson (2010), Goldburd et al. (2016) and, in our tests, performed well in fitting data. We have run a robust estimation with the iteratively reweighted least squares algorithm Holland and Welsch (1977) which, at each iteration, recalculates the weights based on the residual from the previous iteration. This process progressively downweights outliers and iterations continue until the weights converge.

3.4. Numerical implementation

3.4.1. Forecasting the expected value

As explained in Section 2, many candidate models have been tested, but we found that a two-factor model to describe the dynamics of financial log-losses and their volatility is the best compromise between tractability and efficiency. In particular, the novelty of the proposed model (1) consists in a nonzero correlation ρ_t between the two processes x_t and σ_t. Indeed, in contrast with a two-factor Gaussian model, which is more analytically tractable, the two-factor square-root model becomes analytically unmanageable if $\rho_t \neq 0$ (see, for instance, the G2, G2++, CIR2 and CIR2++ models described in Brigo and Mercurio (2006)).
Having said that, if $\rho \neq 0$, no closed formula is known for the transition density of x_t. As a consequence, the conditional expected values of x_t and σ_t cannot be computed explicitly. That means we have to recur to numerical methods in order to produce forecasts within the framework of model (1).
Denote by $X_s = \{X_{s+1}, ...X_{s+N}\},\ s > 0$, a time series of N observed realizations of the process $(x_t)_{t\geq 0}$. Moreover, consider a window, $\mathcal{I}_t$, of fixed size L, that is rolled through time $t \geq 0$. The length of this window is the historical period over which we calibrate our parameter vectors $\nu_t^x := (k_t, \theta_t, \omega_t)$ and $\nu_t^\sigma := (\delta_t, \gamma_t, \eta_t)$, for any time t.
In order to simulate the volatility process σ_t, we construct a time series, V_s, of "pointwise" volatilities, obtained as the pointwise difference in absolute value between X_s and the corresponding exponential moving average (EWMA) E_s, that is

$$V_{s+u} = |X_{s+u} - E_{s+u}|, \quad 1 \leq u \leq N. \tag{14}$$

In our opinion, the above time series is more accurate than other statistics, e.g. the sample standard deviation, because it measures the variability of the process x_t

depending on time.
We use the time series V_s to calibrate the parameter vector ν_t^σ on the rolling window $\mathcal{I}_t$ by applying the maximum likelihood (ML) estimation method, implemented in Matlab, to estimate the parameters of the CIR process Kladıvko (2007). In financial literature, there exists different and more sophisticated methodologies to estimates the parameter of ergodic diffusion processes (see, e.g., (Orlando et al. 2019c, Section 4.4)) but they require rolling windows of size greater than L to be efficient.
Following the algorithm proposed in Kladıvko (2007), the ML estimate $\widehat{\nu}_t^\sigma$ is obtained by solving the following optimization problem

$$\widehat{\nu}_t^\sigma = \arg\big(\max_{\nu_t^\sigma} \ln L(\nu_t^\sigma)\big). \tag{15}$$

Notice that $\ln L(\nu_t^\sigma)$ denotes the log-likelihood function of the CIR process

$$\ln L(\nu_t^\sigma) = \sum_{u=1}^{L-1} \mathcal{P}(V_{s+h+u+1}|V_{s+h+u}) \qquad (h \geq 1),$$

computed on the window $\mathcal{I}_t = \{V_{s+h+1}, ..., V_{s+h+L}\}$, $t = s+h+L$, and $\mathcal{P}$ is the transition density of the CIR process (see (Jeanblanc et al. 2009, Proposition 6.3.2.1)). To ensure the convergence to the ML estimates, the ordinary least-squares (OLS) regression method is used to determine the initial parameter estimates.
The predicted future volatility value σ_{t+u}^F, $u \geq 1$, may be computed by the CIR conditional expectation

$$\sigma_{t+u}^F = \mathbb{E}_{\mathbb{P}}[\sigma_{t+u}|\sigma_t] = \widehat{\theta}_t^\sigma + (V_t - \widehat{\theta}_t^\sigma)e^{-\widehat{k}_t^\sigma u} \qquad (u \geq 1), \tag{16}$$

where V_t is the observed volatility corresponding to σ_t.
The estimate of the parameter vector $\widehat{\nu}_t^x$ on the rolling window $\mathcal{I}_t$ is obtained using the same procedure above-described by using the time series X_s. The sample autocorrelation of X_s on $\mathcal{I}_t$, $\widehat{\rho}_t$, with lag equal to -1, is considered as an estimate of the correlation coefficient ρ_t.
In order to forecast the future value x_{t+u}^F, $u \geq 1$, we applied the second-order Milstein discretization scheme ((Orlando et al. 2019c, Section 4.5)) to simulate the auxiliary process p_t (see (8)) and σ_t observed at m equidistant points in the interval $[t, t+u]$:

$$\begin{cases} \sigma_{t_{i+1}}^S = \sigma_{t_i}^S + \widehat{\delta}_t(\widehat{\gamma}_t - \sigma_{t_i}^S)\Delta + \widehat{\eta}_t\sqrt{\sigma_{t_i}^S \Delta}\, W_{t_i}^\sigma + \frac{\widehat{\eta}_t^2}{4}[(\sqrt{\Delta}\, W_{t_i}^\sigma)^2 - \Delta], \\ p_{t_{i+1}}^S = p_{t_i}^S + h(g^{-1}(p_{t_i}^S + \widehat{\rho}_t f(\sigma_{t_i}^S)), \sigma_{t_i}^S)\Delta + \widehat{\omega}_t\sqrt{\sigma_{t_i}^S(1-\widehat{\rho}_t^2)\Delta}\, B_{t_i} + \frac{(\widehat{\omega}_t \sigma_{t_i}^S (1-\widehat{\rho}_t^2))^2}{4}[(\sqrt{\Delta}\, B_{t_i})^2 - \Delta], \end{cases} \tag{17}$$

where f, g, h are defined by (3), (5), respectively, and $\Delta = t_{i+1} - t_i$ is the time-step, being $t = t_1 < t_2 < ..... < t_m = t + u$. The initial values of the simulated

sample paths has been set $(p_t^S, \sigma_t^S) = (P_t, V_t)$, where (P_t, V_t) denote the corresponding observations in the time series P_s[3] and V_s, respectively.
Following this procedure, we simulated $h = 100,000$ trajectories (p^S, σ^S). Then, the predicted future value p_{t+u}^F, is obtained averaging over the 100,000 corresponding simulated values, that is

$$p_{t+u}^F = \frac{1}{h} \sum_{i=1}^{h} p_{t+u,i}^S. \tag{18}$$

Finally, from relation (9), we get

$$x_{t+u}^F = g^{-1}\big(p_{t+u}^F + \widehat{\rho}_t f(\sigma_{t+u}^F)\big). \tag{19}$$

Note that the Monte Carlo prediction, or equivalently, the (conditioned) expectation used to forecast the future values in formulas (16), (18) and (19) is consistent with the Assumption **??** and the related Proposition 3.2, being $(\sigma_t)_{t\geq 0}$, $(p_t|\sigma_t = \sigma)$ and $(x_t|\sigma_t = \sigma)$ $(\sigma \geq 0)$ a Markov process.

3.4.2. Forecasting the extreme value (VaR)

As tested in Section 4, the forecasted future values provide a good approximation of the expected values of the financial log-losses and the corresponding volatility. To avoid that a future observation will exceed a given high level, an upper bound of predictions x_{t+u}^F is needed ensuring the 99% confidence level Value at Risk (VaR). For this reason we define a correction term as the following random variable

$$z_{t+u} := x_{t+u} - (x_{t+u}^F + \sigma_{t+u}^F), \quad u \geq 1. \tag{20}$$

In other terms, as the distribution of losses is not normal, the correction term z_{t+u} is what we require to get our VaR with a confidence level of 99%. The realization of the random value z_{t+u} is denoted with Z_{t+u} so that the upper bound VaR_{GPD} of the prediction x_{t+u}^F is

$$VaR_{GPD} = x_{t+u}^F + \sigma_{t+u}^F + Z_{t+u}. \tag{21}$$

As we intend to model the extreme values, we assume that Z_{t+u} follows a Generalized Pareto Distribution (GPD), a probability distribution introduced by Pickands Pickands III (1975) as a model for tails. The cumulative distribution function is given by, for all $y > 0$

$$G(y) = \begin{cases} 1 - \left(1 + \frac{\xi y}{\beta}\right)^{-\gamma}, & \text{if } \xi > 0, \\ 1 - e^{-\frac{y}{\beta}}, & \text{if } \xi = 0, \end{cases} \tag{22}$$

[3] $P_s = g(X_s) - \rho_s f(V_s)$.

where ξ, and $\beta > 0$ are the so-called shape and scale parameters, respectively, and $\gamma = 1/\xi$ is the tail index parameter.
To estimate the unknown GPD parameters (ξ, β) we adopted the following procedure. Given the initial rolling window $\mathcal{I}_t = \{X_{s+1}, ...X_{s+L}\}$, where $t = s + L$, used to estimate the parameter vectors ν_t^σ, ν_t^x as above-described, consider a second fixed window $\mathcal{I}'_t = \{X_{s+L+1}, ...X_{s+L'}\}$ with initial size $L' > L$ on which we compute the estimates $(\widehat{\xi}_t, \widehat{\beta}_t)$. Then a realization, Z_{t+u}, of the correction term z_{t+u} is estimated by the sample mean computed over 100,000 simulated random variables with GPD and parameters $(\widehat{\xi}_t, \widehat{\beta}_t)$. Note that in the next steps, while the window $\mathcal{I}_t$ rolls through time, each year adding a new observation and taking off the oldest one, a new observation is added each time to the window $\mathcal{I}'_t$. As a consequence, the size L' of $\mathcal{I}'_t$ increases each time by one year. This is to avoid too large variations in the computation of the correction term that may cause a shortfall of capital for insurers.

3.4.3. Example on earthquake forecasts

As an example, in the following picture Fig. 3, we display the log-losses of the natural disaster (dotted black line). As shown the behaviour is quite erratic and difficult to anticipate. Then, for an insurer, the objective is at least to estimate the expected value over the years. The SMA (in blue) shown here is calculated on the realized occurrences. Then, we show our forecasts (red line) as well as the upper bound (green line). The latter is the VaR for our model (see Sec. 3.2) as obtained through the GPD with the methodology described in Sec. 3.4. Graphically it is possible to see that our model not only is pretty close to the ex post SMA but, also, with a single exception over 119 years, is always above the peaks of realized losses.

In addition to the log-losses, we want to estimate their average volatility. This is of particular importance from a firm standpoint as the aim, is not only to ensure solvency but, also, to deliver a regular stream of cash flow to the shareholders by avoiding excessive variations due to reserves' volatility. Fig. 5 compares the average ex post volatility indicated as SMA (blue line) with our ex ante forecast (red line). Once again, it is possible to see that our forecast is pretty close to the realized volatility.

We recall that we defined Z_t as the correction term to be added to both the occurrences and the volatility. This term changes depending on the size of the windows and influences the values in Tables 5, 6, 9 in Sec. 4. Fig. 6 shows how the correction term can change dramatically when the window is bigger than 50. In our case we opted for a window of size of 20 at that is what we consider a satisfying

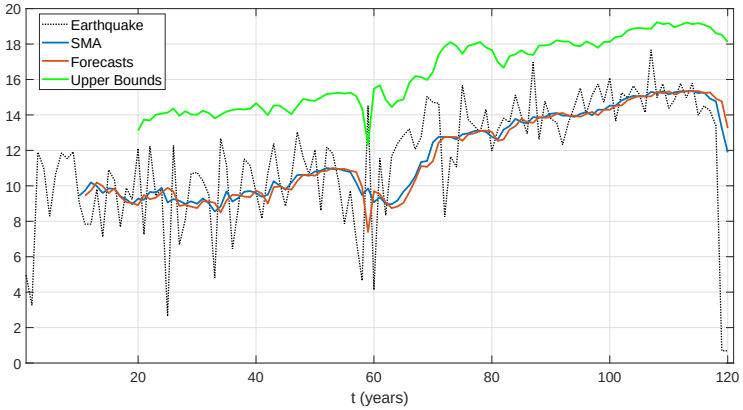

Figure 3: Earthquake Forecasts. The (dotted) black line is the log-losses of the natural disaster X_t, the blue line is its SMA (ex post), the red line represents the corresponding forecasts x_t^F; finally the green line refers to the upper bound VaR_{GPD} computed as $x_t^F + \sigma_t^F + Z_t$ with $L' = 119$. Out of sample forecasts.

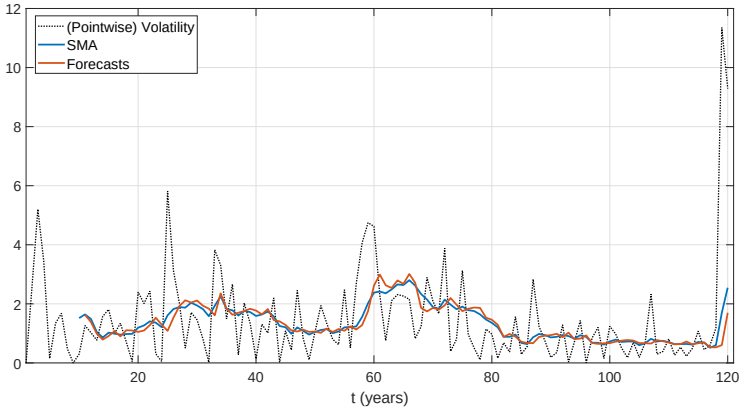

Figure 4: Earthquake volatility Forecasts. The black (dotted) line is the (pointwise) volatility of the log-losses of disaster V_t, the blue line is its SMA (ex post), the red line represents the corresponding forecasts σ_t^F.

Figure 5: Earthquake and its (pointwise) volatility forecasts.

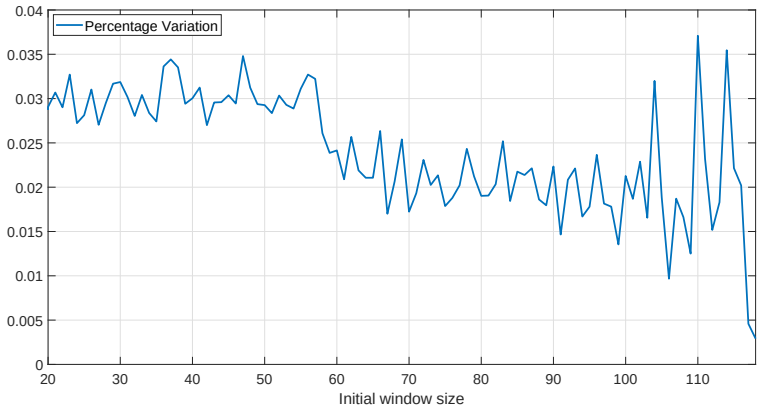

Figure 6: Percentage variation of Z_t for different initial window size $L' \geq 20$, for any $t \geq L'$.

trade-off between size and stability.

Finally, while standard techniques based on extreme value theories produce 5-year forecasts, in Fig. 7 we demonstrate the versatility of our model which is able to preserve its predicting power over longer horizons (e.g. 10 and 15 years).

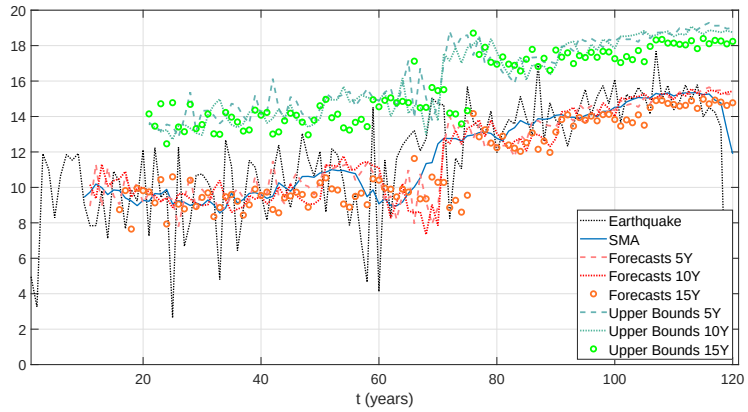

Figure 7: Earthquake log-losses forecasts for the next 5, 10 and 15 years.

3.5. Accuracy statistics for model predictions

As a measure of accuracy we adopt the following statistics:

- The root mean squared error (RMSE), defined as

$$RMSE = \sqrt{\frac{1}{N}\sum_{h=1}^{N} e_h^2}, \tag{23}$$

where e_h denotes the residuals between the observed data and their predictions, over N observations. It captures the closeness between the observed data and the predicted values, in particular values near to zero represent a good result and values near to 1 bad results. Notice that to reduce the effect of the outliers, we use the normalized root mean squared error (NRMSE), defined as follows

$$NRMSE = \frac{RMSE}{X_{max} - X_{min}}, \tag{24}$$

where X_{max} and X_{min} are the maximum and minimum value of the historical time series, respectively.

- The mean absolute percentage error (MAPE), defined below

$$MAPE = \frac{1}{N}\sum_{h=1}^{N}\left|\frac{e_h}{X_h}\right|. \tag{25}$$

Table 4 suggests the accuracy levels about the MAPE criterion.

MAPE	**Forecasting level**
$< 10\%$	High
$10\% - 20\%$	Good
$20\% - 50\%$	Resonable
$> 50\%$	Inaccurate

Table 4: MAPE accuracy levels.

3.6. Backtesting on exceedances for model validation

In order to check if a model is able to meet expected maximum allowed exceptions, we recur the range of tools available to risk management. We said that the upper bound of the GPD represents the maximum loss. Therefore, similarly to what financial institutions do to backtest their VaR, in the following we describe the most popular methods that we are going to use to validate our model.

3.6.1. Traffic Light Test (TLT)

The Traffic Light Test was proposed by the Basel Committee on Banking Supervision 1996, Balthazar (2006) for giving a green light on the adopted model and it is a variant of the binomial test. The TLT test, given a number of exceptions E, calculates the probability of observing from 0 to E exceptions.

3.6.2. Kupiec's POF Test

This test borrows its name from Kupiec (1995) and it is a variant on the binomial test. The Kupiec test is also named proportion of failures (POF) test because the way in which it is constructed. As well as the TLT test, the POF test is based on the binomial distribution but, additionally, it uses a likelihood ratio. This to check if the probability of exceptions is synchronized with the probability p defined by the VaR confidence level. In case the frequency of exceptions over the backtested time series is different than p, the VaR is rejected.

3.6.3. Kupiec's TUFF and TBFI Tests

A second test suggested by Kupiec is called time until first failure (TUFF) Jorion et al. (2009). The TUFF test checks when the first rejection occurs. If that rejection happens (from the probabilistic point of view) too early, the test rejects the VaR. Because the check is limited to the first exception leaves much information out (i.e. what happened after the first exception is ignored) the TBFI test has been developed to include all recorded failures.

3.6.4. Christoffersen's (CC) Interval Forecast Tests

The (CC) Interval Forecast Tests has been proposed by Christoffersen (1998). The idea is to check if the probability of observing an exception at a specific time depends on whether an exception occurred. This test, differently from the unconditional probability of observing an exception, measures only the dependency between consecutive times.

4. Numerical results

4.1. Results on 1-year horizon

In this section we apply the procedure described in Section 3.4 to the Dataset described in Section 3.1. Detailed figures are reported in Section Appendix A. We set the parameters L, L' and Δ equal to

$$L = 10Y, \quad L' = 20Y, \quad \Delta = \frac{1}{360}.$$

As a first step, we computed the NRMSE and MAPE statistics as a difference between the forecasted financial log-losses due to natural disasters and the corresponding simple moving averages (SMA) (Table 5), and between the forecasted volatility and the corresponding simple moving averages (SMA) (Table 6). Further we compare our results with the predictions given by the baseline models. As mentioned the AR(1) and the SMA are indicated to forecast smooth time series. Notice that the calibration of the G2++ model follows the techniques described in Subsection 3.4, where the processes r_t and q_t refer to X_t and V_t, respectively. This because we focus on the variations instead of on the levels with the aim to keep them under control and, so, to avoid unexpected large losses for insures. Notice that the expected log-losses and their volatility are predicted by formula (11) and (12), respectively.

Forecasting error of considered models - Returns						
Horizon	**Model Error**	**Earthquake**	**Storm**	**Flood**	**Drought**	**Ext. Temp.**
	$\text{NRMSE}_{Eq.(1)}$	3.32%	4.80%	4.92%	4.54%	2.44%
	NRMSE_{AR}	24.14%	20.18%	14.30%	17.55%	9.10%
1 Y	NRMSE_{G2}	19.30%	12.46%	15.98%	19.05%	11.21%
	NRMSE_{EVM}	5.79%	4.48%	4.9%	19.05%	10.21%
	NRMSE_{NLP}	17.12%	5.94%	5.36%	7.18%	2.99%
	$\text{MAPE}_{Eq.(1)}$	4.77%	3.02%	5.87%	6.67%	3.02%
	MAPE_{AR}	6.59%	7.14%	18.24%	20.77%	12.16%
1 Y	MAPE_{G2}	7.66%	8.42%	22.78%	21.58%	14.34%
	MAPE_{EVM}	5.23%	3.13%	9.01%	10.23%	6.57%
	MAPE_{NLP}	8.01%	4.20%	13.35%	6.70%	2.91%

Table 5: NRMSE and MAPE between 1 year forecasts of log-losses and their SMA. The gray highlights the results obtained with model in Eq. (1). Out of sample results.

In order to check if the correction term Z_t ensures the 99% confidence level VaR, we consider the percentage variation of the exceeds, for any $t \geq L'$. Indeed, the percentage variation of Z_t check if smooth hedging (i.e., without drastic jumps) holds true for insurance companies. In particular, we analyze the percentage variation and the exceeds for different size L' of the window $\mathcal{J}'_t$, with $L' \geq 20$. Table 8 reports the maximum percentage variation of Z_t and the minimum size L' giving the 99% VaR, for any $t \geq L'$. Moreover, the Kupiec (POF), Christoffersen (CC) and TUFF/TBFI test, at 99% significance level, do not reject their null hypothesis with p-value and

Forecasting error of considered models - Volatility						
Horizon	**Model Error**	**Earthquake**	**Storm**	**Flood**	**Drought**	**Ext. Temp.**
	$\text{NRMSE}_{Eq.(1)}$	8.76%	9.24%	6.55%	9.85%	5.19%
	NRMSE_{AR}	53.10%	37.35%	18.77%	39.43%	44.56%
1 Y	NRMSE_{G2}	24.73%	13.75%	25.48%	45.63%	20.61%
	NRMSE_{EVM}	11.74%	8.49%	6.01%	9.6%	28.80%
	NRMSE_{NLP}	30.12%	24.52%	23.07%	33.45%	23.16%
	$\text{MAPE}_{Eq.(1)}$	5.10%	3.62%	3.60%	7.25%	2.88%
	MAPE_{AR}	11.48%	12.07%	11.13%	20.98%	26.88%
1 Y	MAPE_{G2}	12.13%	11.74%	20.68%	28.94%	10.50%
	MAPE_{EVM}	12.04%	11.71%	8.91%	14.23%	16.72%
	MAPE_{NLP}	35.27%	33.20%	31.31%	48.27%	38.19%

Table 6: NRMSE and MAPE between 1 year forecasts of volatility of log-losses and their SMA. The gray highlights the results obtained with model in Eq. (1). Out of sample results.

L-ratio given in Table 7 [4]; and the traffic light test gives a "green" category with cumulative probability of failures equal to 1.6%.

	POF	**CC**	**TUFF, TBFI**
Response	"accept"	"accept"	"accept"
p-value	0.1542	0.3623	0.4297
L-ratio	2.0301	2.0301	4.0964

Table 7: 99% VaR test response. Out of sample results.

	Earthquake	**Storm**	**Flood**	**Drought**	**Ext. Temp.**
Max. Variation	3.70%	3.25%	4.15%	3.26%	3.55%
Min. L'	61	20	20	23	55

Table 8: Maximum percentage variation of Z_t and minimum L' giving the 99% confidence level VaR. Out of sample results.

[4]Notice that the p-value and L-ratio of the above tests are the same for each time series since they have the same number of observations, same number of exceedances and relative frequency.

4.2. Results on 5-, 10- and 15-year horizon

In addition to 1-year forecasts, to highlight the power of our predictions, we apply the analysis to the next $5Y$, $10Y$ and $15Y$ horizon. As previously done, all forecasts are out of sample. We start with a window of ten data (from $T = 10Y$) and the results are listed in Table 9.
For reason of space, graphs are in Appendix A, where we show the forecasted series (relative to the next year or to 5, 10 and 15 years) $x^F_{t+u}, \sigma^F_{t+u}$ and the percentage variation of Z_t for any natural disaster considered.

Forecasting error of considered models - Returns						
Horizon	**Model Error**	**Earthquake**	**Storm**	**Flood**	**Drought**	**Ext. Temp.**
5 Y	$\text{MAPE}_{Eq.(1)}$	5.10%	6.23%	12.68%	20.60%	20.01%
	MAPE_{AR}	15.46%	14.68%	29.75%	34.34%	22.52%
	MAPE_{G2}	7.79%	8.45%	23.01%	26.70%	20.91%
	MAPE_{EVM}	5.91%	8.03%	22.73%	22.12%	20.84%
	MAPE_{NLP}	6.90%	7.88%	30.84%	24.37%	12.25%
10 Y	$\text{MAPE}_{Eq.(1)}$	5.32%	7.95%	17.60%	29.45%	21.45%
	MAPE_{AR}	16.46%	18.19%	28.75%	38.50%	54.05%
	MAPE_{G2}	7.90%	10.15%	26.59%	29.70%	25.25%
	MAPE_{EVM}	9.16%	12.85%	29.77%	36.91%	23.25%
	MAPE_{NLP}	11.23%	14.49%	46.64%	34.14%	23.95%
15 Y	$\text{MAPE}_{Eq.(1)}$	6.72%	10.25%	19.69%	32.68%	25.15%
	MAPE_{AR}	18.46%	22.19%	29.84%	42.04%	56.27%
	MAPE_{G2}	9.30%	10.92%	27.09%	39.70%	29.34%
	MAPE_{EVM}	11.14%	16.63%	31.99%	38.31%	26.11%
	MAPE_{NLP}	14.47%	28.97%	48.29%	35.42%	39.14%

Table 9: Different MAPE for 5, 10 and 15 years predictions. The gray highlights the results obtained with model in Eq. (1). Out of sample results.

Notice that, as well as illustrated in Tables 5 and 6, we obtained similar results with regard to the volatility and the NRMSE. For the sake of readability we do not show those results.

5. Conclusions

In this work we have presented an original model to forecast (over 1, 5, 10 and 15 years) both the expected value of losses as result of some natural disasters as well as their volatility. To this end we have developed a generalized two-factor square-root model and linked up losses with volatility through stochastic correlation following a Brownian motion. However, while generalized linear models are common instruments for the pricing of non-life insurance contracts Laudagé et al. (2019), they are inadequate for extreme claims. For this reason, to quantify the maximum loss in terms of Value at Risk (VaR), we employed a Generalized Pareto Distribution (GPD). The performance of our model was compared with four baseline models (i.e. AR, G2++, EVT and NLP) in terms of accuracy. Exceedances over the forecasted VaR (that in our case is the upper bound of the GDP) were backtested. The result is that our model compares well with respect to the benchmarks (forecasting efficiency) and that backtests confirm the goodness of the chosen VaR (model validation). More in general, this methodology applies as well to dramatic changes of a given line of business (LOB) due to unexpected events such as COVID-19.

6. Conflict of interest

The authors declare no conflict of interest

References

Acar, S. and Natcheva-Acar, K. (2009). A guide on the implementation of the Heath-Jarrow-Morton two-factor Gaussian short rate model (HJM-G2++). Technical Report 170, Fraunhofer (ITWM).

Ahlip, R., Park, L. A., and Prodan, A. (2017). Pricing currency options in the Heston/CIR double exponential jump-diffusion model. *International Journal of Financial Engineering*, 4(01):1750013.

Alvarez-Ramirez, J., Alvarez, J., Rodriguez, E., and Fernandez-Anaya, G. (2008). Time-varying Hurst exponent for US stock markets. *Physica A: statistical mechanics and its applications*, 387(24):6159–6169.

Bacry, E., Mastromatteo, I., and Muzy, J.-F. (2015). Hawkes processes in finance. *Market Microstructure and Liquidity*, 1(01):1550005.

Balthazar, L. (2006). The regulation of market risk: The 1996 amendment. In *From Basel 1 to Basel 3: The Integration of State-of-the-Art Risk Modeling in Banking Regulation*, pages 23–31. Springer.

Basel Committee (1996). Supervisory framework for the use of backtesting in conjunction with the internal models approach to market risk capital requirements. *Basel Committee on Banking and Supervision, Switzerland*.

Bollerslev, T. (1986). Generalized autoregressive conditional heteroskedasticity. *Journal of econometrics*, 31(3):307–327.

Böttcher, B., Schilling, R., and Wang, J. (2013). A primer on Feller semigroups and Feller processes. In *Lévy Matters III*, pages 1–30. Springer.

Brigo, D. and Mercurio, F. (2006). *Interest rate models-theory and practice: with smile, inflation and credit*. Springer-Verlag: Berlin, Heidelberg.

Bufalo, M., Mininni, R. M., and Romanelli, S. (2019). A semigroup approach to generalized Black-Scholes type equations in incomplete markets. *Journal of Mathematical Analysis and Applications*, 477(2):1195–1223.

Cai, J.-J., Wan, P., and Ozel, G. (2020). Parametric and non-parametric estimation of extreme earthquake event: the joint tail inference for mainshocks and aftershocks. *Extremes*, pages 1–16.

Carbone, A., Castelli, G., and Stanley, H. E. (2004). Time-dependent hurst exponent in financial time series. *Physica A: Statistical Mechanics and its Applications*, 344(1-2):267–271.

Chavas, D., Yonekura, E., Karamperidou, C., Cavanaugh, N., and Serafin, K. (2013). Us hurricanes and economic damage: Extreme value perspective. *Natural Hazards Review*, 14(4):237–246.

Chen, J., Lei, X., Zhang, L., and Peng, B. (2015). Using extreme value theory approaches to forecast the probability of outbreak of highly pathogenic influenza in Zhejiang, China. *PloS one*, 10(2):e0118521.

Christoffersen, P., Heston, S., and Jacobs, K. (2009). The shape and term structure of the index option smirk: Why multifactor stochastic volatility models work so well. *Management Science*, 55(12):1914–1932.

Christoffersen, P. F. (1998). Evaluating interval forecasts. *International economic review*, pages 841–862.

Coles, S., Bawa, J., Trenner, L., and Dorazio, P. (2001). *An introduction to statistical modeling of extreme values*, volume 208. Springer.

Cox, S. H., Lin, Y., and Pedersen, H. (2010). Mortality risk modeling: Applications to insurance securitization. *Insurance: Mathematics and Economics*, 46(1):242–253.

CRED (2020). CRED's Emergency Events Database (EM-DAT). `https://www.emdat.be/`. Accessed: 2020-01-03.

De Jong, P. and Heller, G. Z. (2008). *Generalized linear models for insurance data*. Cambridge University Press.

Eichler, M., Dahlhaus, R., and Dueck, J. (2017). Graphical modeling for multivariate hawkes processes with nonparametric link functions. *Journal of Time Series Analysis*, 38(2):225–242.

Embrechts, P., Liniger, T., and Lin, L. (2011). Multivariate hawkes processes: an application to financial data. *Journal of Applied Probability*, 48(A):367–378.

Engel, K.-J. and Nagel, R. (2001). One-parameter semigroups for linear evolution equations. In *Semigroup forum*, volume 63, pages 278–280. Springer.

Ewald, C.-O., Zhang, A., and Zong, Z. (2019). On the calibration of the Schwartz two-factor model to WTI crude oil options and the extended Kalman filter. *Annals of Operations Research*, 282(1-2):119–130.

Faff, R. and Treepongkaruna, S. (2013). A re-examination of the empirical performance of the Longstaff and Schwartz two-factor term structure model using real yield data. *Australian Journal of Management*, 38(2):333–352.

Goldburd, M., Khare, A., and Tevet, D. (2016). *Generalized linear models for insurance rating*. Number 5. Casualty Actuarial Society, CAS Monographs Series.

Goldstein, G. R., Goldstein, J. A., Mininni, R. M., and Romanelli, S. (2016). The semigroup governing the generalized Cox-Ingersoll-Ross equation. *Advances in Differential Equations*, 21(3/4):235–264.

Goldstein, J. (1985). *Semigroups of Linear Operators and Applications*. University Press, Oxford, New York.

Hall, E. C. and Willett, R. M. (2016). Tracking dynamic point processes on networks. *IEEE Transactions on Information Theory*, 62(7):4327–4346.

Hanafy, M. et al. (2020). Application of Generalized Pareto in Non-Life Insurance. *Journal of Financial Risk Management*, 9(03):334.

Hawkes, A. G. (2018). Hawkes processes and their applications to finance: a review. *Quantitative Finance*, 18(2):193–198.

Heston, S. L. (1993). A closed-form solution for options with stochastic volatility with applications to bond and currency options. *The review of financial studies*, 6(2):327–343.

Holland, P. W. and Welsch, R. E. (1977). Robust regression using iteratively reweighted least-squares. *Communications in Statistics-theory and Methods*, 6(9):813–827.

Hsieh, P.-H. (2004). A data-analytic method for forecasting next record catastrophe loss. *Journal of risk and insurance*, 71(2):309–322.

Hull, J. C. and White, A. D. (1994). Numerical procedures for implementing term structure models II: two-factor models. *The Journal of Derivatives*, 2(2):37–48.

Hurst, H. E. (1956). Methods of using long-term storage in reservoirs. *Proceedings of the Institution of Civil Engineers*, 5(5):519–543.

Jeanblanc, M., Yor, M., and Chesney, M. (2009). *Mathematical Methods for Financial Markets*. Springer Finance. Springer-Verlag, London.

Jin, J.-L., Cheng, J., and Wei, Y.-M. (2008). Forecasting flood disasters using an accelerated genetic algorithm: Examples of two case studies for China. *Natural Hazards*, 44(1):85–92.

Jorion, P. et al. (2009). *Financial risk manager handbook*, volume 406. John Wiley & Sons.

Karatzas, I. and Shreve, S. (2012). *Brownian motion and stochastic calculus*. Springer Science & Business Media.

Kladıvko, K. (2007). Maximum likelihood estimation of the Cox-Ingersoll-Ross process: the Matlab implementation. *Technical Computing Prague*.

Kohrs, H., Mühlichen, H., Auer, B. R., and Schuhmacher, F. (2019). Pricing and risk of swing contracts in natural gas markets. *Review of Derivatives Research*, 22(1):77–167.

Kupiec, P. (1995). Techniques for verifying the accuracy of risk measurement models. *The Journal of Derivatives*, 3(2).

Laudagé, C., Desmettre, S., and Wenzel, J. (2019). Severity modeling of extreme insurance claims for tariffication. *Insurance: Mathematics and Economics*, 88:77–92.

Longstaff, F. A. and Schwartz, E. S. (1992). Interest rate volatility and the term structure: A two-factor general equilibrium model. *The Journal of Finance*, 47(4):1259–1282.

Mandelbrot, B. B. and Van Ness, J. W. (1968). Fractional Brownian motions, fractional noises and applications. *SIAM review*, 10(4):422–437.

Mandelbrot, B. B. and Wallis, J. R. (1969). Robustness of the rescaled range r/s in the measurement of noncyclic long run statistical dependence. *Water resources research*, 5(5):967–988.

Martins, A. L. A., Liska, G. R., Beijo, L. A., de Menezes, F. S., and Cirillo, M. Â. (2020). Generalized Pareto distribution applied to the analysis of maximum rainfall events in Uruguaiana, RS, Brazil. *SN Applied Sciences*, 2(9):1–13.

Nawrocki, D. (1995). R/S analysis and long term dependence in stock market indices. *Managerial finance*, 21:78–78.

Nelder, J. A. and Wedderburn, R. W. (1972). Generalized linear models. *Journal of the Royal Statistical Society: Series A (General)*, 135(3):370–384.

Ogata, Y. (1988). Statistical models for earthquake occurrences and residual analysis for point processes. *Journal of the American Statistical association*, 83(401):9–27.

Ohlsson, E. and Johansson, B. (2010). *Non-life insurance pricing with generalized linear models*, volume 174. Springer.

Oksendal, B. (2013). *Stochastic differential equations: an introduction with applications*. Springer Science & Business Media.

Orlando, G., Mininni, R. M., and Bufalo, M. (2018). *A new approach to CIR short-term rates modelling*, pages 35–44. Springer International (USA).

Orlando, G., Mininni, R. M., and Bufalo, M. (2019a). A new approach to forecast market interest rates through the CIR model. *Studies in Economics and Finance*.

Orlando, G., Mininni, R. M., and Bufalo, M. (2019b). Forecasting interest rates through Vasicek and CIR models: a partitioning approach. *Journal of Forecasting*.

Orlando, G., Mininni, R. M., and Bufalo, M. (2019c). Interest rates calibration with a CIR model. *The Journal of Risk Finance*.

Pickands III, J. (1975). Statistical inference using extreme order statistics. *The Annals of Statistics*, 3(1):119–131.

Povinelli, R. J. (2000). Identifying temporal patterns for characterization and prediction of financial time series events. In *International Workshop on Temporal, Spatial, and Spatio-Temporal Data Mining*, pages 46–61. Springer.

Qian, B. and Rasheed, K. (2004). Hurst exponent and financial market predictability. In *IASTED conference on Financial Engineering and Applications*, pages 203–209.

Recchioni, M. C. and Sun, Y. (2016). An explicitly solvable Heston model with stochastic interest rate. *European Journal of Operational Research*, 249(1):359–377.

Rouah, F. D. (2013). *The Heston Model and Its Extensions in Matlab and C*. John Wiley & Sons.

Rypdal, M. and Løvsletten, O. (2013). Modeling electricity spot prices using mean-reverting multifractal processes. *Physica A: Statistical Mechanics and its Applications*, 392(1):194–207.

Shang, J. and Sun, M. (2019). Geometric hawkes processes with graph convolutional recurrent neural networks. In *Proceedings of the AAAI Conference on Artificial Intelligence*, volume 33, pages 4878–4885.

Shreve, S. E. (2004). *Stochastic calculus for finance II: Continuous-time models*, volume 11. Springer Science & Business Media.

Taira, K. (1984). Diffusion processes and partial differential equations. In *North-Holland Mathematics Studies*, volume 98, pages 197–210. Elsevier.

Tsuchiya, O. (2019). Two-factor Hull-White model revisited: correlation structure for two-factor interest rate model in CVA calculation. *Available at SSRN 3338987*.

Utsu, T. (1970). Aftershocks and earthquake statistics (i): Some parameters which characterize an aftershock sequence and their interrelations. *Journal of the Faculty of Science, Series 7, Geophysics*, 3(3):129–195.

Vyushin, D., Kushner, P., and Zwiers, F. (2012). Modeling and understanding persistence of climate variability. *Journal of Geophysical Research: Atmospheres*, 117(D21).

Zivot, E. (2009). Practical issues in the analysis of univariate GARCH models. In *Handbook of financial time series*, pages 113–155. Springer.

Appendix A. Graphical evidences

In this section we report some figures showing the out of sample results we obtained with our model. For each type of natural disaster first we show the expected loss alongside with the upper bound of our estimate (i.e. a sort of forecasted worst case). Then, as the insurer needs to keep under control the volatility of the losses, we also display the pointwise volatility. See Figures A.8, A.11, A.14, A.17.

After that we show the variation of z_t and, finally, the forecasts with different time horizon (5, 10 and 15 years) jointly with their related upper bounds. The latter with the usual intent to keep the exceedances under control. See Figures A.9, A.10, A.12, A.13, A.15, A.16, A.18, A.19.

As documented, all figures support the validity of the proposed model.

Appendix A.1. Storm

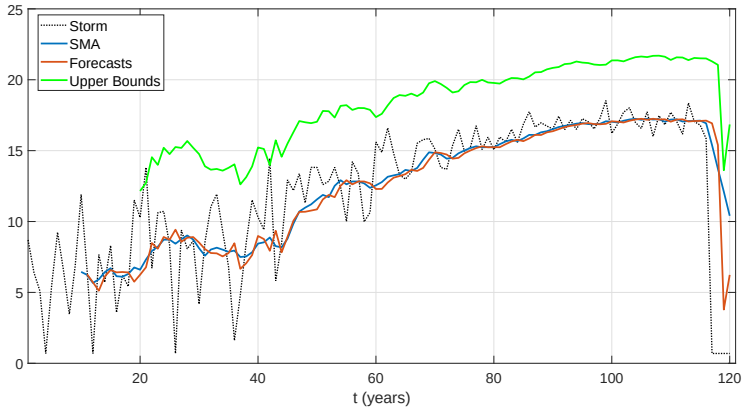

(a) Storm Forecasts. The (dotted) black line is the log-losses of the natural disaster X_t, the blue line is its SMA (ex post), the red line represents the corresponding forecasts x_t^F; finally the green line refers to the upper bound VaR_{GPD} computed as $x_t^F + \sigma_t^F + Z_t$ with $L' = 119$. Out of sample forecasts.

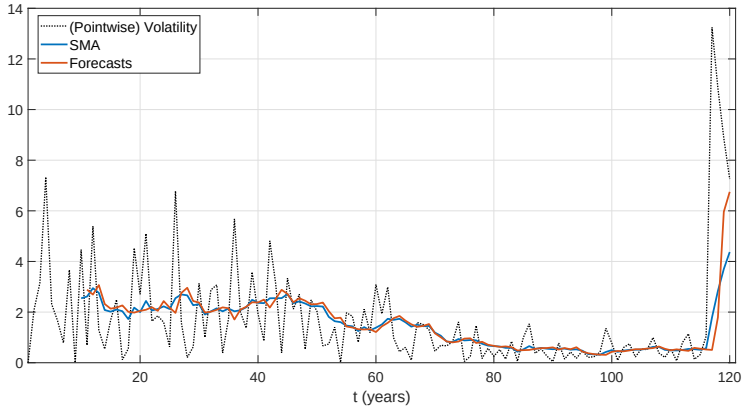

(b) Storm volatility Forecasts. The black (dotted) line is the (pointwise) volatility of the log-losses of disaster V_t, the blue line is its SMA (ex post), the red line represents the corresponding forecasts σ_t^F.

Figure A.8: Storm and its (pointwise) volatility forecasts.

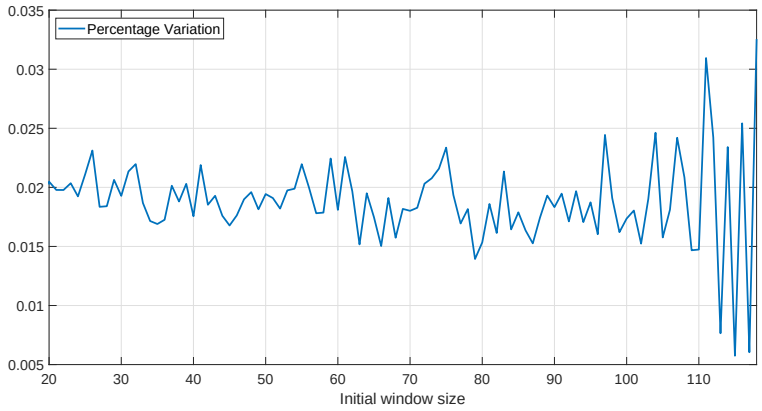

Figure A.9: Percentage variation of Z_t for different initial window size $L' \geq 20$, for any $t \geq L'$.

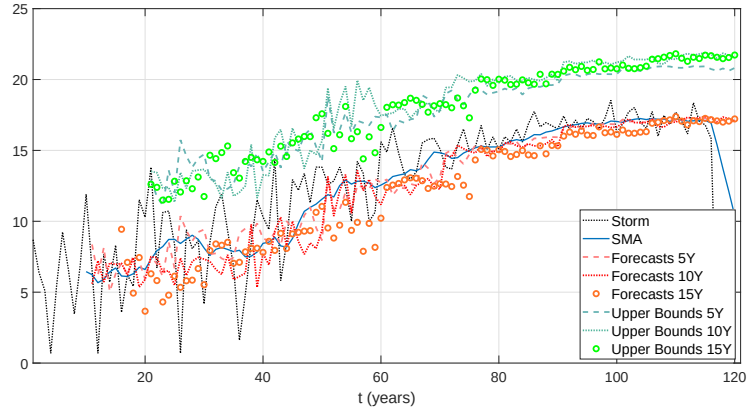

Figure A.10: Storm log-losses forecasts for the next 5, 10 and 15 years.

Appendix A.2. Flood

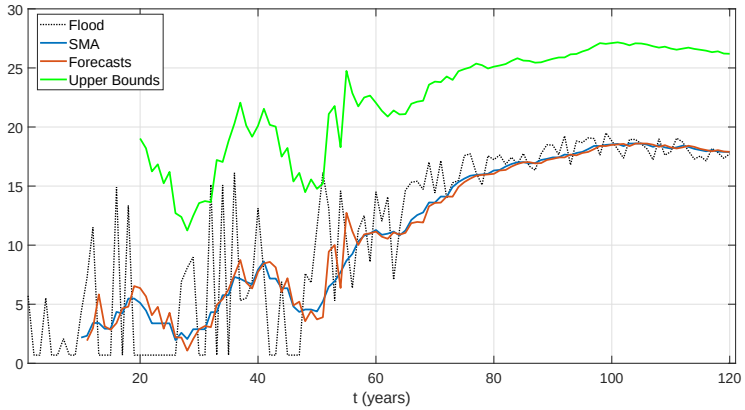

(a) Flood Forecasts. The (dotted) black line is the log-losses of the natural disaster X_t, the blue line is its SMA (ex post), the red line represents the corresponding forecasts x_t^F; finally the green line refers to the upper bound VaR_{GPD} computed as $x_t^F + \sigma_t^F + Z_t$ with $L' = 119$. Out of sample forecasts.

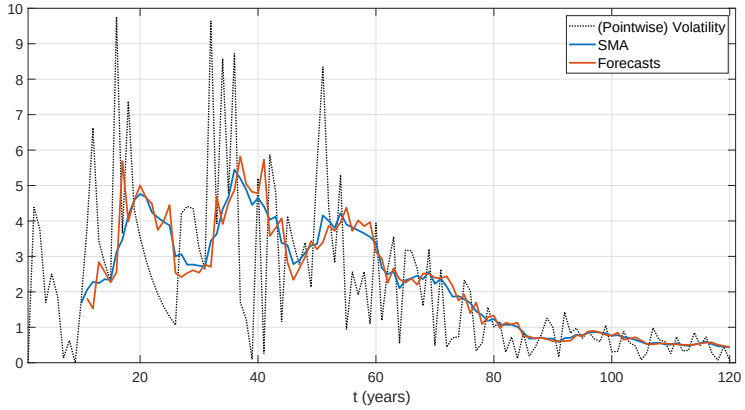

(b) Flood volatility Forecasts. The black (dotted) line is the (pointwise) volatility of the log-losses of disaster V_t, the blue line is its SMA (ex post), the red line represents the corresponding forecasts σ_t^F.

Figure A.11: Flood and its (pointwise) volatility forecasts.

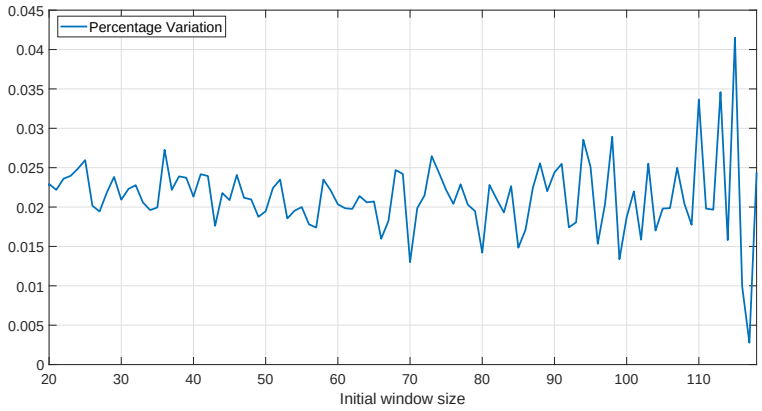

Figure A.12: Percentage variation of Z_t for different initial window size $L' \geq 20$, for any $t \geq L'$.

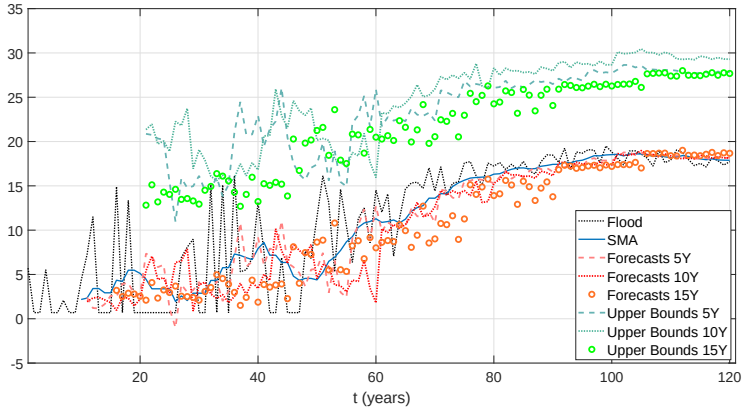

Figure A.13: Flood log-losses forecasts for the next 5, 10 and 15 years.

Appendix A.3. Drought

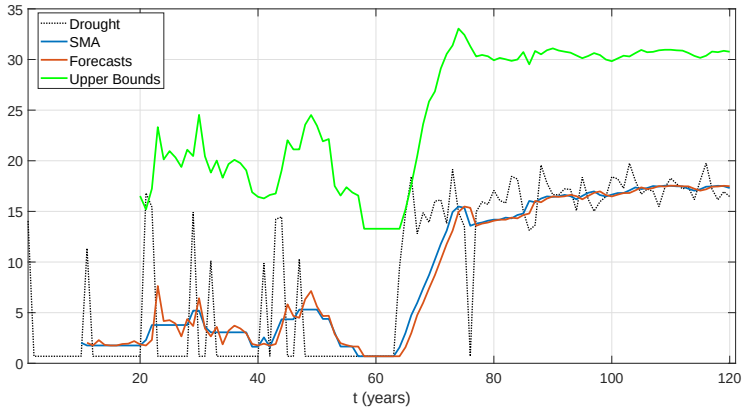

(a) Drought Forecasts. The (dotted) black line is the log-losses of the natural disaster X_t, the blue line is its SMA (ex post), the red line represents the corresponding forecasts x_t^F; finally the green line refers to the upper bound VaR_{GPD} computed as $x_t^F + \sigma_t^F + Z_t$ with $L' = 119$. Out of sample forecasts.

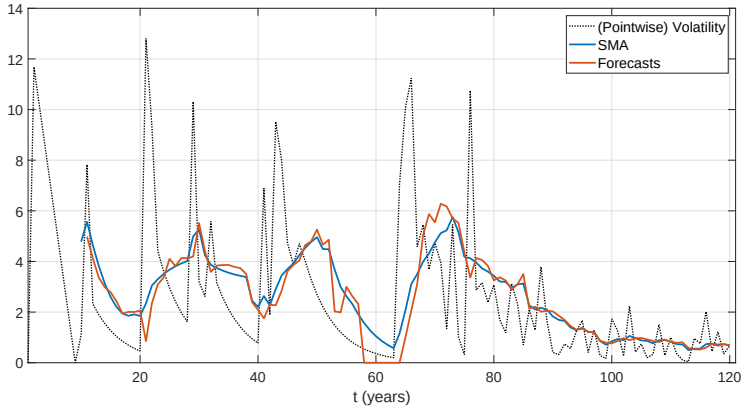

(b) Drought volatility Forecasts. The black (dotted) line is the (pointwise) volatility of the log-losses of disaster V_t, the blue line is its SMA (ex post), the red line represents the corresponding forecasts σ_t^F.

Figure A.14: Drought and its (pointwise) volatility forecasts.

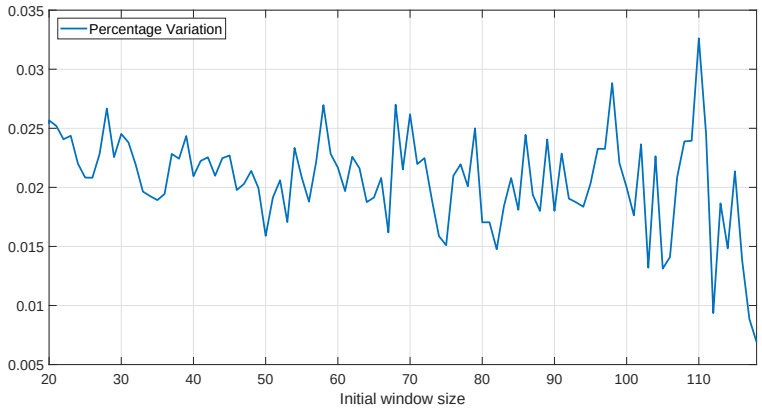

Figure A.15: Percentage variation of Z_t for different initial window size $L' \geq 20$, for any $t \geq L'$.

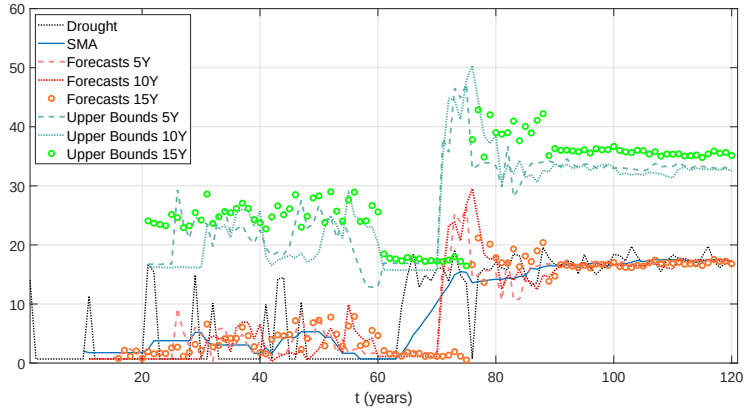

Figure A.16: Drought log-losses forecasts for the next 5, 10 and 15 years.

Appendix A.4. Extreme temperature

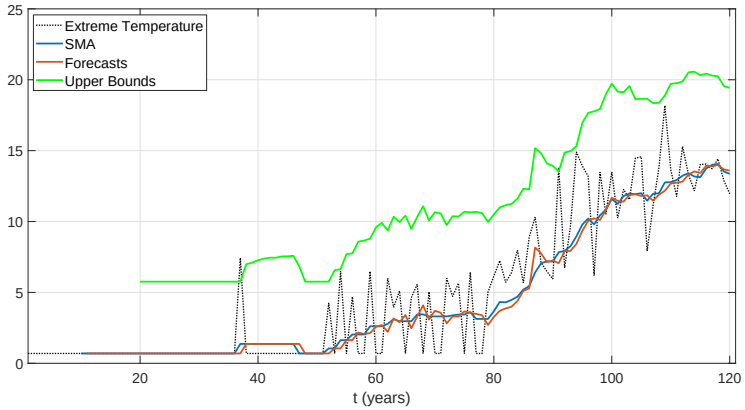

(a) Extreme temperature Forecasts. The (dotted) black line is the log-losses of the natural disaster X_t, the blue line is its SMA (ex post), the red line represents the corresponding forecasts x_t^F; finally the green line refers to the upper bound VaR_{GPD} computed as $x_t^F + \sigma_t^F + Z_t$ with $L' = 119$. Out of sample forecasts.

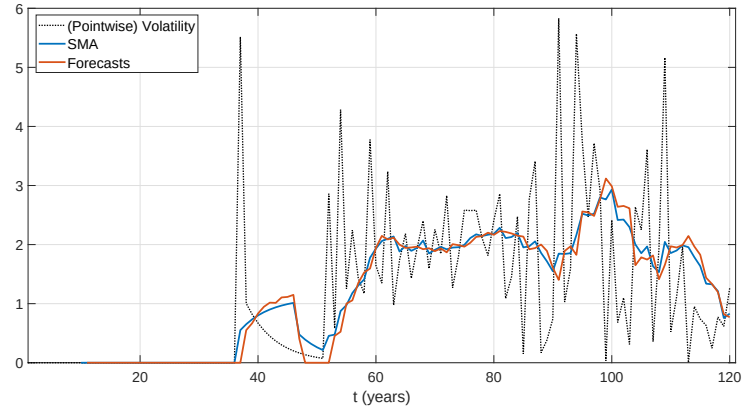

(b) Extreme temperature volatility Forecasts. The black (dotted) line is the (pointwise) volatility of the log-losses of disaster V_t, the blue line is its SMA (ex post), the red line represents the corresponding forecasts σ_t^F.

Figure A.17: Extreme temperature and its (pointwise) volatility forecasts.

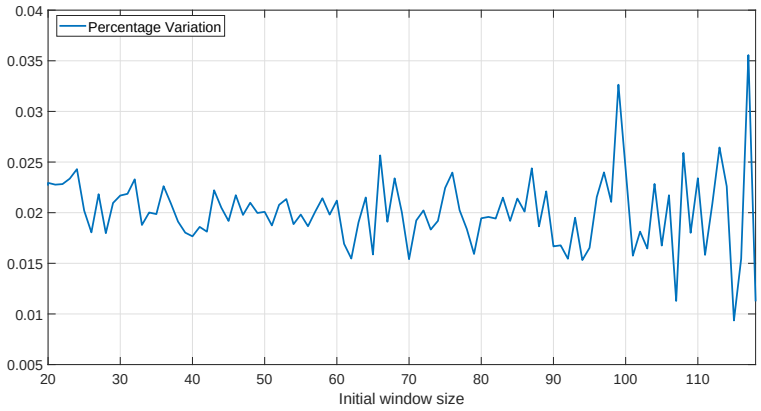

Figure A.18: Percentage variation of Z_t for different initial window size $L' \geq 20$, for any $t \geq L'$.

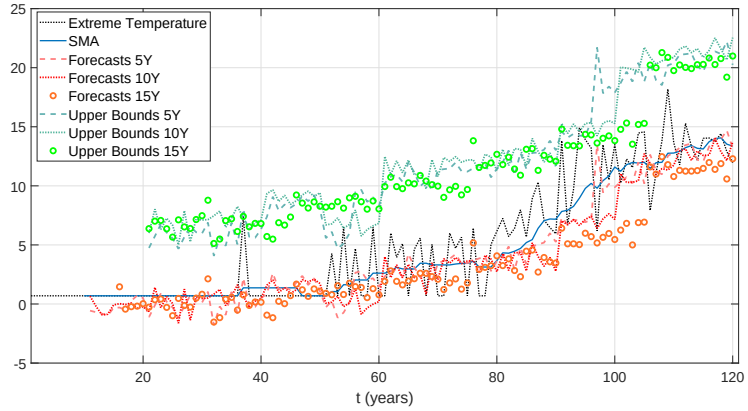

Figure A.19: Extreme Temperature log-losses forecasts for the next 5, 10 and 15 years.

Climate Risks for Sovereign Debt

Andrea Consiglio
University of Palermo
andrea.consiglio@unipa.it

Stavros A. Zenios
University of Cyprus National Academy of Sciences, Letters, and Arts
Bruegel
zenios.stavros@ucy.ac.cy

Extended abstract [1]

We integrate state-of-the-art stochastic Debt Sustainability Analysis (DSA) with a climate Integrated Assessment Model (IAM) to evaluate the impact of climate changes to estimate the risks to sovereigns from climate change and allows for the estimation of potential fiscal space to deal with mitigation and adaptation costs. We employ the scenario matrix architecture developed by the IPCC (The Intergovernmental Panel on Climate Change), looking at narrative scenarios of plausible combinations of greenhouse-gas concentrations (RCP, Representative Concentration Pathway) with pathways of economic and social developments (SSP, Shared Socioeconomic Pathways). See for more details. We work with the RICE50+ [3] that considers anthropogenic greenhouse gas emissions in climate systems and climate change impacts on social-economic systems, to obtain forward-looking projections of GDP growth, potential economic damages and per-capita GDP. We then conduct DSA using a stochastic portfolio optimization model (DebtRisk) [2] using RICE50+ output as baseline GDP growth. The DSA produces a fan-chart of the two key vulnerability indicators used by the International Monetary Fund and the European Stability Mechanism: Debt-to-GDP ratio (stock, D/Y) and Gross Financing Needs (flow, GFN/Y). These fan charts extend several years into the future and are summarised by percentiles. Our final aim is to build a vulnerability map to show how the climate changes will impact debt dynamics with a given probability score.

[1] Speaker:Andrea Consiglio, andrea.consiglio@unipa.it.

Keywords
Debt sustainability analysis; Integrated assessment models; Climate risks.

References

[1] Zenios, S.A. (2021) "The risks from climate change to sovereign debt in Europe", Policy Contribution 16/2021, Bruegel.

[2] Stavros A. Zenios, Andrea Consiglio, Marialena Athanasopoulou, Edmund Moshammer, Angel Gavilan, Aitor Erce. "Risk Management for Sustainable Sovereign Debt Financing". Operations Research, 69(3):755-773.

[3] Paolo Gazzotti, Johannes Emmerling, Giacomo Marangoni, Andrea Castelletti, Kaj-Ivar van der Wijst, Andries Hof and Massimo Tavoni. "Persistent inequality in economically optimal climate policies". Nature Communications, 12,3421 (2021).

A replication of Pindyck's willingness to pay: on the efforts required to obtain results

Luca Gerotto
Department of Economics and Finance,
Università Cattolica del Sacro Cuore;
Department of Economics,
Ca' Foscari University of Venice.
luca.gerotto@unicatt.it

Paolo Pellizzari
Department of Economics,
Ca' Foscari University of Venice.
paolop@unive.it

Extended abstract [1]

This paper presents a verification and an extension - as defined in Clemens [1] - of the study entitled "Uncertain outcomes and climate change policy" by R.S. Pindyck, *J. Environ. Econ. Manag.* Pindyck [2] can be interpreted as a very simplified integrated assessment model (IAM) for the analysis of climate change. The model incorporates the distribution of (uncertain) temperature change and the distribution of the (uncertain) impact of this change on the growth of consumption, and computes willingness to pay (WTP), i.e. "the fraction of consumption ... that society would be willing to sacrifice, now and throughout the future, to ensure that any increase in temperature at a specific horizon H is limited to τ." These fractions are typically below 2%; Pindyck [2] states that this is consistent with the adoption of a moderate abatement policy.

Replication is of paramount importance in science, and lies at the very heart of what differentiates science from cheap talk and non-scientific arguments. There is a growing awareness of the need for more replication

[1] Session: Climate risk and Integrated assessment models for economics and finance
Speaker: Paolo Pellizzari, paolop@unive.it.

studies; too many scholars have sadly admitted faltering or failed attempts to reproduce other researchers' work; see Baker [3].

In several cases, our verification analysis confirms the results and the associated economic interpretation. However, those results cannot be replicated in one out of five cases. The replication is therefore only partially successful: the numerical results for some sets of parameter values turn out to be overly sensitive to a variety of technical computational settings. This suggests that great caution is needed with regard to estimates and policy conclusions based on this model. A re-estimation of the model using more recent climate data, which suggest that temperature increase is now higher on average but less widely dispersed, does not lead to significant economic differences in the results.

Keywords
Numerical replication; Numerical integration; Climate change; Economic impact; Uncertainty.

References

[1] M.A. Clemens, The meaning of failed replications: A review and proposal, J. Econ. Surv., **31(1)**(2017), 326–342.

[2] R.S. Pindyck, Uncertain outcomes and climate change policy, J. Environ. Econ. Manag., **63(3)**(2012), 289–303.

[3] M. Baker, 1,500 scientists lift the lid on reproducibility, Nature, **533(7604)**(2016), 452–454.

Measuring Basis Risk in Weather Index Insurance: hybrid parametric solutions

Maria Carannante and Valeria D'Amato
Department of Pharmacy,
University of Salerno
Italy
mcarannante@unisa.it, vdamato@unisa.it

Paola Fersini
Department of Business and Management,
Luiss "Guido Carli" University,
Italy
pfersini@luiss.it

Salvatore Forte
Department of Business and Management,
Università Telematica Giustino Fortunato,
Italy
s.forte@unifortunato.eu

Extended abstract

Climate change is one of the most important challenges to face relating to weather risk management, in particular for agriculture and energy sectors. In recent years, adverse weather events changed in severity and frequency [1] in such a way that the traditional statistical instruments, based on extreme value theory, are not yet adequate to assess the risk. From a quantitative point of view, the challenge is to identify analytical tools that allow quantifying the risks in an effective way, exploiting the availability of huge public databases, such as satellite or sensors' data, and the ability to process them, offered by artificial intelligence as previously proposed by Biffs and Chavez [2]. In this sense, satellite data and machine learning algorithms make weather index insurance a valid hedging tool in the agricultural sector [3]. However, since this type of hedging is subject to basis risk, it is

necessary to define how to measure it, to evaluate the effectiveness of the hedging position. Our approach consists of the construction of a parametric insurance contract based on weather index that allows mitigating the basis risk through the use of satellite data and a "dynamic" random forest algorithm, also comparing bagging and boosting algorithms [4], that allows handling time-series data maintaining the temporal structure in the trees. The parametric insurance will be based on the combination of two bioclimatic indices, considering the joint distribution with respect to extreme and non-extreme events, following the insurance contracts proposed by Salgueiro [5], and customizing the insurance parameters on the basis of particular soil conditions or of the premium rate. To do this, a theoretical framework and a quantification of basis risk for weather index insurance are also proposed.

Keywords
Weather Index Insurance; Satellite Data; Basis Risk; Machine Learning; Parametric Insurance.

References

[1] SwissRe Institute, *Natural catastrophes in times of economic accumulation and climate change*, Sigma No 2/2020, 2020

[2] E. Biffis, E. Chavez, Satellite Data and Machine Learning for Weather Risk Management and Food Security, Risk Analysis, **37**(2020), 1508-1521

[3] World Bank, *Weather Index Insurance for Agriculture: Guidance for Development Practitioners*, Agriculture and Rural Development Discussion Paper; 50. World Bank, Washington, DC, 2011

[4] T. Chen, C. Guestrin, XGBoost: A Scalable Tree Boosting System, Proceedings of the 22nd ACM SIGKDD International Conference on Knowledge Discovery and Data Mining, New York, NY, USA: ACM, 785–794

[5] A.M. Salgueiro, Weather index-based insurance as a meteorological risk management alternative in viticulture, Wine Economics and Policy, **8**(2019), 114-126